Numerical Study of Unsteady Viscous Flow past a Lifting Plate

ROBERT A. SCHMALL* AND ROBERT B. KINNEY†
University of Arizona, Tucson, Ariz.

Numerical predictions are made for the unsteady two-dimensional viscous flow past a finite flat plate at angle of attack. The flow is analyzed from the standpoint of vorticity production and transport using the complete vorticity transport equation. The entire fluid motion is ultimately calculated through application of the velocity induction law (Law of Biot-Savart). Fundamental to the approach is the specification of "bound" and "sheet" vortex distributions at the plate location. These are so constituted that the surface adherence condition appropriate to the viscous flow is satisfied. The analysis shows how the vortex distributions arise, their interrelationship, and their effect on the developing rotational flow about the plate. Results are first presented for a low Reynolds number flow ($Re = 4$) at zero angle of attack. These are followed by results for the plate at 30° angle of attack for Reynolds numbers of 4 and 400. The flow simulation is found to be very good, and to whatever extent possible, the results are compared with those from earlier works based on conventional approaches involving the stream function. The comparisons are quite satisfactory.

Nomenclature

B_p = series coefficients in expression for γ, Eq. (5)
K = time-function of integration in expression for γ
L = cord length of the plate
m = summation index in Eq. (13)
n = number of time increments
Re = Reynolds number, UL/ν
t = time
U = velocity of the undisturbed fluid
u = velocity component parallel to the plate
v = velocity component transverse to the plate
X = dummy variable of integration
x = coordinate measured parallel to the plate from the midcord
Y = dummy variable of integration
y = coordinate measured transverse from the plate
α = angle of attack of the plate, Fig. 1
γ = bound vorticity distribution along the plate cord
θ = polar angle, Fig. 1
ν = kinematic viscosity
ξ = dummy variable of integration
Ω = total free vorticity in the fluid
ω = free vorticity distribution in the fluid
Δ = finite increment

Superscripts
$+$ = upper surface of the plate
$-$ = lower surface of the plate

Subscripts
b = contribution to the velocity from the bound vorticity (boundary property)
f = contribution to the velocity from the free vorticity (fluid property)
i,j = node indices in the x, y directions

Introduction

THE long list of recent contributions to computational fluid dynamics[1] is evidence of the growing interest in the subject. The book by Roache[2] gives an excellent orientation to the subject plus a description of the many existing numerical approaches. With few exceptions, the accepted techniques for calculating unsteady two-dimensional flows are based on the dynamical and kinematical relationship between the vorticity and stream function. Differences are due primarily to the choice of implicit vs explicit time methods, representation of the spatial derivatives, and implementation of the vorticity boundary condition at solid surfaces. Although some important features of the methods have yet to be investigated, including their transportive, conservative, and stability properties, it does appear that the conceptual foundations have been fully established.

Departing from past conventions, Lighthill[3] has outlined a fundamentally different approach for the calculation of unsteady incompressible viscous flows. Although the basic flow variable is still the vorticity, this being in common with other methods, dependence on the stream function is completely eliminated. Instead, the velocity field is computed from the velocity induction law, also known as the Law of Biot-Savart. Whereas this law is encountered most frequently in connection with inviscid flows, it is purely kinematical in nature, and therefore, it is valid for nonsteady viscous as well as inviscid flows.

Fundamental to Lighthill's approach is the calculation of the vorticity production at solid surfaces. To obtain this, the Biot-Savart Law is first used to calculate the velocity field everywhere in the fluid at some instant of time. It is then recognized that the velocities thus obtained need not satisfy the viscous adherence condition at solid boundaries. In particular, there may be a slip-component tangential to the surface. When this occurs, new total vorticity must instantaneously appear at the surface in just such measure that the velocity field due to this new vorticity, when combined with that previously determined, reduces the slip velocity to zero. This new vorticity forms a vortex sheet, the local strength of which is given by the local tangential slip velocity. The slip velocity, then, is a measure of the vorticity production at solid surfaces. However, the manner in which this quantity is incorporated into the subsequent calculation of the new vorticity field is subject to some interpretation. One scheme for doing this has already been used by Paolino[4] and Kinney and Paolino[5] in their numerical predictions for the unsteady flow near the leading edge of a semi-infinite flat plate. An extension of this same scheme has been used in the present work and will be described in the later sections.

Recent Related Work

During the course of this investigation, Wu and Thompson[6] and Chorin[7] have reported numerical approaches which are remarkably similar to that described by Lighthill.[3] Each make

Received March 4, 1974; revision received June 3, 1974. The authors express their appreciation to the Computer Center of the University of Arizona for providing access to the CDC 6400 digital computer. This work was partially supported by the National Science Foundation under Grant GK-40006.

Index categories: Viscous Nonboundary-Layer Flows; Nonsteady Aerodynamics.

* Environmental Engineer, presently with Public Service Company of New Mexico, Albuquerque, N. Mex.

† Associate Professor of Aerospace and Mechanical Engineering. Member AIAA.

use of the Biot-Savart Law as well as the vorticity transport equation. However, differences do exist in the implementation of the vorticity boundary condition at solid surfaces. This, of course, is one of the most critical aspects of any computational procedure.

Wu and Thompson[6] first calculate the velocities at points in the fluid from the Biot-Savart Law. Using these values in conjunction with the velocity boundary conditions (prescribed on each of the boundary cells adjacent to the solid surface), the vorticity inside the boundary cell is obtained from a finite-difference representation of the curl of the velocity vector. In so doing, it is especially critical that the boundary vorticity maintain zero normal velocities at all points on the surface. This boundary value for the vorticity is then used in the solution of the vorticity transport equation. Two flow examples are treated. For the first example, in which the symmetrical flow about an infinite plate is calculated, the normal velocity at the plate is automatically zero. Therefore, it does not enter into the determination of the boundary vorticity, which is simply equal to the velocity obtained at the node point above the plate divided by the vertical node spacing. The situation is quite different for their second example, however, in which the two-dimensional flow about a circular cylinder is treated. Unfortunately, no details are given in the paper as to how the curl of the velocity vector (and thus the boundary vorticity) is actually obtained, but a total of fifteen different schemes were evaluated before a final choice was made.

Chorin[7] presents a method which looks very promising for treating two-dimensional viscous flows at high Reynolds numbers. Although there are many interesting aspects to his approach, discussion here will be limited to the implementation of the vorticity boundary condition. For a given vorticity field in the fluid, the Biot-Savart Law is used to obtain the normal component of velocity induced at points along the solid boundary. The boundary points are centred on a finite number of segments covering the outline of the solid body. A potential velocity field is then constructed which has the negative value of this normal velocity at the boundary points. When the potential velocity field is added to the rotational velocity field because of the fluid vorticity, the resultant fluid motion appears to slip tangentially over the surface. Thus, maintenance of a zero normal velocity at the surface is guaranteed. The apparent slip velocity is next computed at the boundary points. Up to this point, the concept is essentially as outlined by Lighthill.[5] Enforcement of the zero slip condition causes total vorticity to appear at the boundary in the form of a vortex sheet. The boundary vorticity, which by the way occupies the entire boundary-layer thickness (presumed to be thin because of the high Reynolds number), has a local value equal to the product of the slip velocity and the length of the boundary segment from which it originates. In a broad sense, the sheet vorticity specifies the boundary value for the vorticity which is eventually transported throughout the fluid by convection and diffusion. Inherent in this approach is the requirement that the boundary-layer thickness on the body be infinitesimal, but allowance is made for a rotational wake-development behind the body. The method is used to calculate the two-dimensional flow past a circular cylinder, and the results are in good accord with those from previous studies.

Problem Statement and Theoretical Approach

In the present paper, numerical predictions are made for the unsteady two-dimensional flow past a lifting plate. The plate is infinitesimal in thickness but finite in length. It is initially at rest in a motionless, incompressible, and unbounded viscous fluid. At some instant in time, the plate is impulsively accelerated to a finite velocity which is maintained constant thereafter. The velocity vector of the plate makes an angle with the plate cord. In a coordinate scheme fixed to the plate, the fluid appears to flow past the plate which is maintained at a specified angle of attack to the freestream. The angle of attack and Reynolds number are parameters to be varied in the calculations, and the flow development is to be followed as a function of time. Only one previous study by Lugt and Haussling[8] is known to the authors which treats a similar flow problem. They analyzed the unsteady two-dimensional flow past a thin elliptic airfoil, rather than a flat plate. Also, they employed the more conventional vorticity-stream function approach.

In the present paper, the vorticity concepts originally outlined by Lighthill[3] and discussed above are used as the basis for the numerical calculations. Attention is focused here on the low to moderate Reynolds number range for which the vorticity layer adjacent to the plate has appreciable thickness. Thus, in contrast to Chorin's[7] work, the details of the flow very near the body are important.

In order to analyse the flow, a bound vortex is placed coincident with the plate cord. The bound vortex is so distributed as to insure that the normal velocity component of the fluid at the plate is zero for all time. Thus, the bound vortex plays the same role as the potential-velocity function used by Chorin,[7] but no counterpart exists in the approach used by Wu and Thompson.[6] The tangential adherence condition is satisfied by interposing vortex sheets between the fluid and the upper and lower surfaces of the plate. The vortex sheets act as distributed surface sources (or sinks) for the vorticity which ultimately enters the fluid by diffusion.

As pointed out by Batchelor,[9] the analogy between vorticity and heat diffusion is quite close, particularly in two dimensions. The kinematic viscosity ν is analogous to the fluid thermal conductivity. Thus, $-\nu\partial\omega/\partial y$ represents the molecular flux of total vorticity in the y-direction. At the plate, where the fluid velocity must be zero, this term describes the transverse flux of total vorticity from the plate into the fluid. This vorticity is subsequently transported throughout the fluid and is termed the "free" vorticity. The "bound" vorticity, which occupies the location of the plate, is never released to the fluid.

It remains to relate the vortex sheet strength to the surface flux of free vorticity into the fluid. On this point, Lighthill is not explicit, and some interpretation is necessary. In this work, the apparent slip velocity is first calculated at points along the plate due to the bound and free vortex distributions. This is in accordance with Chorin.[7] This slip velocity then specifies the amount of new free vorticity which must subsequently enter the fluid during a small time interval Δt. This defines the essential boundary condition which must be used in the solution of the vorticity transport equation. The boundary condition does not involve the vorticity itself at solid surfaces, nor even its normal derivative. Rather, the boundary value specified is the integral over an incremental time of the normal derivative of the free vorticity evaluated at the surface. An explicit expression for this boundary condition plus other details pertinent to the analysis are given in the next section.

Analysis

A Cartesian coordinate system is fixed to the plate at mid-cord, and the angle of the plate relative to its direction of motion is denoted by α (see Fig. 1). In the chosen reference frame, the plate of length L appears to be stationary, and the speed of the undisturbed fluid is given by U. The flow is assumed to be two dimensional.

Initially, the free vorticity of the fluid is zero, but after some time has elapsed, a rotational fluid layer develops near the plate. The free vorticity in this layer is governed by the unsteady equation

$$\frac{\partial\omega}{\partial t}+\frac{\partial}{\partial x}(u\omega)+\frac{\partial}{\partial y}(v\omega)=\frac{1}{Re}\left(\frac{\partial^2\omega}{\partial x^2}+\frac{\partial^2\omega}{\partial y^2}\right) \tag{1}$$

where all the variables have been made dimensionless by U and L.

Because of the unsymmetrical flowfield, the free vorticity associated with the fluid can induce a net normal component of velocity at locations along the plate cord. Let this normal

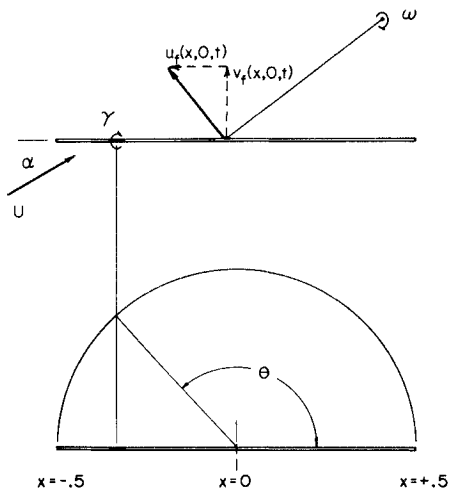

Fig. 1 Schematic diagram of the flow configuration and coordinate system.

velocity relative to the plate be denoted by $v_f(x,0,t)$, where the subscript f is a reminder that this is the contribution from the free vorticity. Applying the velocity induction law (Biot-Savart Law), one obtains

$$v_f(x,0,t) = \frac{1}{2\pi}\int_{-\infty}^{+\infty}\int_{-\infty}^{+\infty}\frac{(X-x)\omega(X,Y,t)}{(X-x)^2+Y^2}\,dX\,dY \qquad (2)$$

In our convention, ω is positive in the clockwise direction. It should also be mentioned that a tangential velocity component is generally induced at the plate as well. This will be discussed at a later point in the analysis.

Since a relative normal velocity cannot be tolerated at the plate surface, a distribution of bound vorticity $\gamma(x,t)$ is superimposed along the plate cord. The velocity field of this must be sufficient to just cancel $v_f(x,0,t)$ plus the freestream velocity component, $\sin\alpha$. One thus obtains the following integral relationship for γ:

$$\frac{1}{2\pi}\int_{-1/2}^{+1/2}\frac{\gamma(\xi,t)\,d\xi}{(x-\xi)} = v_f(x,0,t)+\sin\alpha \qquad (3)$$

where the right-hand side of Eq. (3) is considered known. Also, γ is taken to be positive in the clockwise direction.

At this point it is interesting to note that $v_f(x,0,t)$ plays the same role as the derivative of the camber function in thin-airfoil theory.[10] Indeed, for purposes of applying viscous-fluid corrections to ideal-fluid calculations, it can be envisioned that the viscous fluid adjacent to the plate "induces" camber on the flat airfoil.

Adopting the classical procedure for obtaining γ from Eq. (3), one finds

$$\gamma(\theta,t) = -[B_0(t)+2\sin\alpha]\frac{\cos\theta}{\sin\theta} - \frac{K(t)}{\sin\theta} + 2\sum_{p=1}^{\infty}B_p(t)\sin(p\theta)$$

where (4)

$$B_p(t) = \frac{2}{\pi}\int_0^{\pi} v_f(\theta,0,t)\cos(p\theta)\,d\theta, \quad (p=0,1,2,\ldots) \qquad (5)$$

In the foregoing, $K(t)$ is an arbitrary function of integration, and θ is related to x by the transformation $x=\frac{1}{2}\cos\theta$. It can thus be seen that γ is implicitly dependent on the field of free vorticity through the constants B_p. It will be shown subsequently that the function $K(t)$ is dependent on the surface generation of free vorticity at the plate.

In steady ideal-fluid flat-airfoil theory, K is a constant which is usually determined from the Kutta condition. This condition requires that $\gamma=0$ at $\theta=0$ (i.e., the fluid leaves smoothly from the trailing edge of the plate). However, this condition cannot be imposed in this unsteady analysis. Rather, K is determined from the stronger requirement that the total vorticity (free plus bound) be zero at every instant of time. That is,

$$\int_{-1/2}^{+1/2}\gamma(x,t)\,dx + \int_{-\infty}^{+\infty}\int_{-\infty}^{+\infty}\omega(X,Y,t)\,dX\,dY = 0 \qquad (6)$$

Denoting the double integral of free vorticity in the foregoing by Ω, and after integrating the expression for γ over the plate cord, one obtains from Eq. (6)

$$K(t) = [2\Omega(t)/\pi]+B_1(t) \qquad (7)$$

This rather simple result is a consequence of the orthogonality of the trigonometric functions over the interval 0 to π.

Although in some instances Ω can be evaluated from the integration of ω over the entire flowfield, it is more general to make use of the fact that all of the free vorticity in the fluid has originated from the plate surface. Since in dimensional notation $-\nu\partial\omega/\partial y$ evaluated at $y=0$ denotes the surface flux of total free vorticity from the plate into the fluid, one can write the equivalent expression for Ω as follows:

$$\Omega(t) = -\frac{1}{Re}\int_{-1/2}^{1/2}\int_0^t\left[\frac{\partial\omega}{\partial y}(x',0^+,t')-\frac{\partial\omega}{\partial y}(x',0^-,t')\right]dt'\,dx' \qquad (8)$$

where care has been taken to separate the contributions from the upper ($y=0^+$) and lower ($y=0^-$) portions of the plate. Also, the variables appearing in Eq. (8) have been made non-dimensional. The technique used to evaluate $\Omega(t)$ will be outlined at a later point in the analysis.

The development thus far has been concerned with the construction of the bound vorticity field such that the plate condition on the transverse velocity component is satisfied. We now turn our attention to the satisfaction of the adherence condition as applied to the u component of the velocity.

Just as ω can induce a v component of velocity at the plate, so can it induce a u component of velocity as well. One obtains for this contribution

$$u_f(x,0,t) = -\frac{1}{2\pi}\int_{-\infty}^{+\infty}\int_{-\infty}^{+\infty}\frac{Y\omega(X,Y,t)}{(x-X)^2+Y^2}\,dX\,dY \qquad (9)$$

In addition, there is associated with the bound vorticity an apparent tangential velocity discontinuity across the plate. That is,

$$u_b(x,0^+,t)-u_b(x,0^-,t) = \gamma(x,t) \qquad (10)$$

From aerodynamic theory, it is known further that $u_b(x,0^+,t) = -u_b(x,0^-,t)$, from which it follows that $u_b(x,0^\pm,t) = \pm\frac{1}{2}\gamma(x,t)$. When the two contributions, u_f and u_b, are added to the x component of the freestream velocity, "apparent" slip velocities exist on the upper and lower surfaces as follows:

$$u_{\text{slip}}(x,0^+,t) = \cos\alpha+u_f(x,0,t)+\tfrac{1}{2}\gamma(x,t) \qquad (11a)$$

$$u_{\text{slip}}(x,0^-,t) = \cos\alpha+u_f(x,0,t)-\tfrac{1}{2}\gamma(x,t) \qquad (11b)$$

No distinction is made for the upper and lower surfaces when specifying $u_f(x,0,t)$, since it is the same at each location. From Eq. (11), it is seen that $\gamma(x,t)$ still represents the difference between the apparent slip velocities on the upper and lower surfaces.

The right-hand members of Eq. (11) contain all known quantities. In general, their sum will not be zero. Since a tangential velocity-slip at the plate cannot be tolerated in a viscous flow analysis, the "apparent" slip must be eliminated by interposing vortex sheets between the fluid and the plate surfaces. The velocity field of the upper and lower sheets must be sufficient to reduce both slip components to zero. Thus, the vortex sheet strengths are given, respectively, by $u_{\text{slip}}(x,0^+,t)$ and $u_{\text{slip}}(x,0^-,t)$.

As pointed out by Lighthill,[3] the two vortex sheets give rise to a surface flow of free vorticity into the fluid. This is expressed by

$$-\frac{1}{Re}\int_t^{t+\Delta t}\frac{\partial\omega}{\partial y}(x,0^+,t')dt' = u_{\text{slip}}(x,0^+,t) \qquad (12)$$

An analogous relationship holds for the bottom surface. This important result shows that the local slip velocity at any time t determines the amount of new free vorticity per unit area of

the plate which enters the fluid in the subsequent time increment Δt. The only restriction is that Δt be sufficiently small that this new vorticity is confined to a very thin layer adjacent to the plate. Equation (12) is the essential boundary condition to be used in the numerical solution of Eq. (1).

In applying Eq. (12), the sign convention adopted here is important to keep in mind. For a positive slip velocity on the upper surface, positive (clockwise) free vorticity is generated. On the other hand, a positive slip velocity on the lower surface generates negative free vorticity. The sign of the slip velocity is thus important in determining which portions of the plate act as vorticity sources and which act as vorticity sinks. Lighthill[3] has emphasized that a vorticity-source region, followed downstream by a sink region, is usually a precursor to flow separation (perhaps better called flow stagnation for unsteady, low Reynolds number flows).

Equation (12) provides a convenient means for evaluating the amount of free vorticity, and thus $\Omega(t)$, in the fluid at any time. If $t = n\Delta t$, where n is the number of time increments elapsed, one has from Eq. (8)

$$\Omega(n\Delta t) = \sum_{m=0}^{n-1} \left\{ \int_{-1/2}^{1/2} [u_{\text{slip}}(x, 0^+, m\Delta t) - u_{\text{slip}}(x, 0^-, m\Delta t)]\, dx \right\} \tag{13}$$

with $\Omega(0) = 0$. It is important to note that the summation proceeds over $n-1$ time steps. Also, in view of Eq. (11), the integrand of Eq. (13) is equivalent to $\gamma(x, m\Delta t)$.

It remains only to specify the velocity at points in the fluid. The x component of velocity is obtained from the velocity induction law as follows:

$$u(x, y, t) = \cos\alpha + \frac{1}{2\pi} \left\{ \int_{-\infty}^{+\infty} \int_{-\infty}^{+\infty} \frac{(y-Y)\omega(X, Y, t)}{(x-X)^2 + (y-Y)^2}\, dX\, dY + \int_{-1/2}^{1/2} \frac{y\gamma(\xi, t)}{(x-\xi)^2 + y^2}\, d\xi \right\} \tag{14}$$

This can be recognized as a generalization of Eq. (11) for $y \neq 0$. Although $v(x, y, t)$ can be obtained in an analogous manner, it is more straightforward to use the equation of continuity once $u(x, y, t)$ is known.

This completes the analytical framework. The numerical scheme used to solve the foregoing equations will be presented in a later section. Before turning to this, however, it will be helpful to describe a typical calculation cycle.

Computational Procedure

The solution scheme will be described for the general flow configuration with $\alpha \neq 0$. At zero angle of attack, the procedure is greatly simplified, as will be shown at the end of this section.

The fluid and plate are initially at rest. At $t = 0 + \varepsilon$, $\varepsilon \ll \Delta t$, the plate is moved impulsively to the left. Initially the free vorticity of the fluid is zero, and thus $v_f(x, 0, \varepsilon)$ and $u_f(x, 0, \varepsilon)$ are zero. From Eqs. (4, 5, 7, and 13), $K(\varepsilon)$ is zero, and $\gamma(x, \varepsilon)$ is the same as that obtained for potential flow past a nonlifting plate. The apparent slip velocities can be evaluated from Eq. (11), following which Eq. (12) is used to determine the amount of free vorticity which enters the fluid from the plate surface during the first time increment Δt. This is the essential boundary condition needed to start the solution of Eq. (1). The velocity components appearing in Eq. (1) are those corresponding to potential flow past a nonlifting plate.

Suppose now that some time t has elapsed, and the fluid is permeated with free vorticity. All flow variables, including the apparent slip velocity at the plate are known. The procedure is as follows:

1) From Eq. (12) and its counterpart on the lower surface, the total flow of free vorticity during the next time increment Δt is obtained per unit area of the plate surface.

2) Since the velocity field must be determined simultaneously with the vorticity field, estimates for u and v are used in the integration of Eq. (1). These are taken to be the velocity components at the previous time t. With these and the prescribed surface flow of free vorticity, an estimate of the free vorticity field is obtained at $t+\Delta t$ by integrating Eq. (1).

3) The quantities v_f and u_f, from Eqs. (2) and (9), respectively, are next calculated.

4) The quantity Ω is obtained from Eq. (13), this requiring only a knowledge of the distribution for γ up through the time t.

5) The B_p's are evaluated next, so that with Eq. (7), the distribution of γ at the current time can be obtained.

6) Having obtained γ, a better estimate of the velocity field in the fluid at $t+\Delta t$ can be determined from Eq. (14) plus the continuity equation.

7) This new velocity field is then used to obtain a new estimate for ω at $t+\Delta t$ through an integration of Eq. (1). However, in carrying out this step, the surface flow of free vorticity over the time interval is not changed from that determined in step 1 at the start of the computational cycle. That is, the surface generation of free vorticity is completely specified by the flow conditions at time t, and this does not change during the iteration process.

8) Having then obtained a better estimate of ω at $t+\Delta t$, the calculations are repeated in the above manner for as many iterations as necessary. The number of iterations is usually dictated by the size of the time step Δt. In these studies, the time step is so chosen that two sweeps through the calculation cycle are sufficient.

The calculations are considerably simplified when the plate is at zero angle of attack (nonlifting plate). In particular, γ is identically zero for all time. The calculation procedure only involves steps 1–3 (with $v_f = 0$ because of flow symmetry), 6, and 7. This reduces to the procedures adopted by Kinney and Paolino[5] in their study of symmetrical flow past a semi-infinite flat plate.

Numerical Methods

A system of node points is superimposed on the fluid surrounding the plate, and around each node a control volume of unit depth into the plane of flow is constructed. Let Δx_i and Δy_j denote the dimensions of the control volume in the plane at the i–j node. In this case, i and j, respectively, identify the location of each node in the x- and y-coordinates. For the present calculations, $1 \leqq i \leqq 75$ and $1 \leqq j \leqq 30$. The leading and trailing edges of the plate are, respectively, located midway between i nodes 19 and 20, and 39 and 40. Also, the plate cord is midway between j nodes 15 and 16.

As a matter of convenience, the Δx_i dimension was fixed throughout the flowfield at 0.05 (the plate length is 1). The Δy_j dimension is not a constant but expands outward from above the plate according to the relationship $\Delta y_j = 1.03\Delta y_{j-1}$ (for $j \geqq 17$) and similarly for below the plate. The choice of the smallest Δy dimension nearest the plate surface depends on the

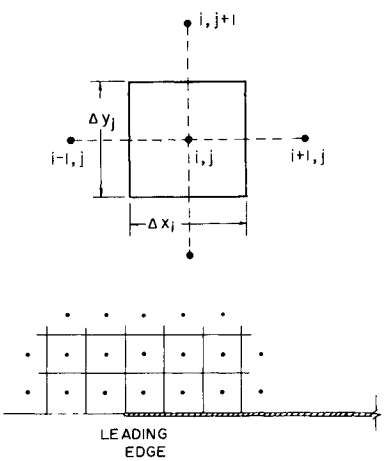

Fig. 2 Typical node-arrangement relative to the plate surface.

Reynolds number. For subsequent calculations performed with $Re = 4$, this value was 0.05, whereas for $Re = 400$, the value 0.0125 was assigned.

Each node point is centered within each control volume. A representative arrangement of nodes and control volumes near the plate is depicted in Fig. 2. A vorticity balance is next performed on each control volume in the fluid at the instant of time $(n+\frac{1}{2})\Delta t$. One obtains for a typical node interior to the flow (for constant Δx_i)

$$\left[\frac{\partial\omega}{\partial t}\right]_{i,j}^{n+1/2}\Delta y_j\Delta x_i = [\tfrac{1}{2}(u_{i-1,j}+u_{i,j})\omega_{i-1,j}]^{n+1/2}\Delta y_j + [\omega_{i-1,j}-2\omega_{i,j}+\omega_{i+1,j}]^{n+1/2}\frac{\Delta y_j}{Re\,\Delta x_i} + [v_{i,j-1/2}\omega_{i,j-1}]^{n+1/2}\Delta x_i + [\omega_{i,j-1}-\omega_{i,j}]^{n+1/2}\times\frac{2\Delta x_i}{Re(\Delta y_j+\Delta y_{j-1})} - [\tfrac{1}{2}(u_{i,j}+u_{i+1,j})\omega_{i,j}]^{n+1/2}\Delta y_j - [v_{i,j+1/2}\omega_{i,j}]^{n+1/2}\Delta x_i - [\omega_{i,j}-\omega_{i,j+1}]^{n+1/2}\times\frac{2\Delta x_i}{Re\,(\Delta y_{j+1}+\Delta y_j)} \quad (15)$$

In the foregoing, $v_{i,j-1/2}$ and $v_{i,j+1/2}$ denote, respectively, the transverse velocities at the control surfaces between nodes $j-1$ and j, and $j+1$ and j.

It will be recognized that the present scheme uses an "upwind differencing" method for the convection terms (assuming u and v are positive). This has been used previously by Gentry, Martin, and Daly.[11] For regions of the flow in which u and v are negative, the appropriate modification to Eq. (15) is made in order to preserve this feature.

One then introduces the following approximations

$$\left[\frac{\partial\omega}{\partial t}\right]_{i,j}^{n+1/2} = \frac{\omega_{i,j}^{n+1}-\omega_{i,j}^{n}}{\Delta t} \quad (16)$$

$$[u_{i-1,j}\omega_{i-1,j}]^{n+1/2} = \tfrac{1}{2}\{[u_{i-1,j}\omega_{i-1,j}]^{n+1}+[u_{i-1,j}\omega_{i-1,j}]^{n}\} \quad (17)$$

and so on for each of the terms ‡ in Eq. (15). Boundary conditions are imposed on the free vorticity beyond the periphery of the computational grid. In this study, the vorticity outside the grid is set equal to zero. The u and v components of velocity just beyond the computational grid are set equal to their values corresponding to potential flow past a nonlifting plate. For the present study, this choice is immaterial since the calculations were terminated before the vorticity at the outer fringes of the grid increased significantly above zero. If appreciable vorticity had been convected past the downstream boundary, the specification of the velocities there would have been handled differently.

In view of the flow of free vorticity from the plate surface into the fluid, Eq. (15) was modified as follows for $j = 14$ and $20 \leq i \leq 39$. The last two terms on the right-hand side were replaced by $(\Delta x_i/\Delta t)u_{\text{slip}}(x^i, 0^-, n\Delta t)$. For $j = 15$, a similar deletion was made to the third and fourth terms, and $(\Delta x_i/\Delta t)u_{\text{slip}}(x_i, 0^+, n\Delta t)$ was inserted, where the apparent slip velocities were obtained from Eq. (11). This assured that the proper amount of free vorticity entered the fluid elements adjacent to the upper and lower surfaces of the plate.

After Eq. (15) is written for each node, there results a set of simultaneous equations for the free vorticity at each node point for the time $(n+1)\Delta t$. The nonhomogeneous portion contains all the flow variables at the previous time $n\Delta t$. The system of equations was solved by successive iterations using the Gauss-Seidel method.

It still remains to outline the calculation procedure used for the distribution of bound vorticity and the velocity field. The essential ingredient to the determination of the bound vorticity is the normal velocity component at the plate which is induced by the free vorticity, Eq. (2). This was obtained by first integrating the free vorticity with respect to x, holding y fixed. The vorticity was assumed to vary linearly with x between adjacent nodes. The result can be expressed as a finite sum involving natural logarithms and arctangents. The integration was next performed in the y direction using a semi-open quadrature formula based on the trapezoidal rule. These steps are quite straightforward, and length limitations preclude a more complete development here. More details can be found in the dissertation[12] on which this paper is based.

The calculation of the B_p's was carried out using a linear variation for v_f (as a function of θ) between adjacent nodes along the plate and integrating the result analytically. The first 25 such coefficients were obtained and found to be sufficient to define the series contribution to the bound vorticity. The quantity K appearing in Eq. (4) was obtained at time $(n+1)\Delta t$ using Eqs. (7) and (13). To evaluate Eq. (13), the apparent slip velocities are needed only up through the time $n\Delta t$. These are given by Eq. (11). The numerical integration with respect to x was carried out using an open-interval modification of the trapezoidal rule.

The u components of velocity were obtained from Eq. (14) using the same procedure to evaluate the double integral as that described above in the calculation of v_f. The integration of the bound vorticity proceeded similarly with a linear approximation for γ being made between adjacent x nodes.

The v component of velocity needed at the upper and lower surfaces of the control volume in the flow was obtained from mass continuity once the u components were calculated. One thus has

$$v_{i,j+1/2} = v_{i,j-1/2}+(\Delta y_i/2\Delta x_i)(u_{i+1,j}-u_{i-1,j}) \quad (18)$$

Known values for $v_{i,j-1/2}$ were first obtained along the entire x axis. For that portion which coincides with the plate, this velocity was set equal to zero. Upstream and downstream of the leading and trailing edges, this velocity was calculated to be the sum of the contributions due to the angle of attack and that induced by the bound and free vorticities. The procedure

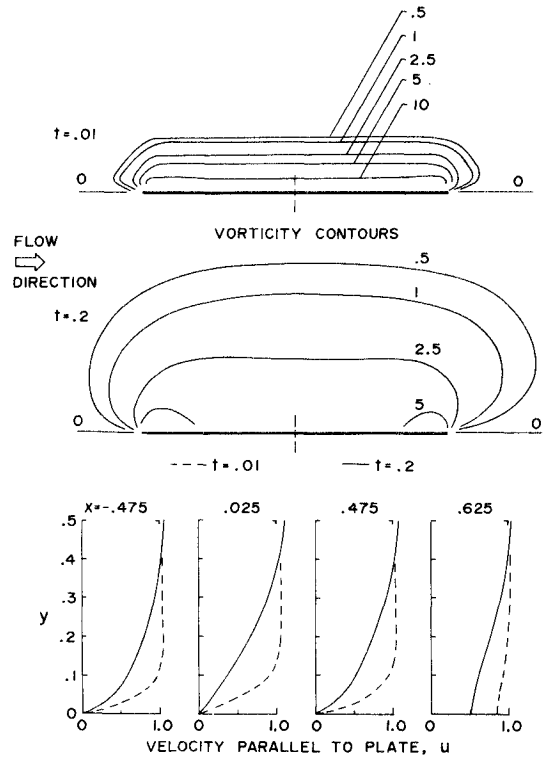

Fig. 3 Contours of constant vorticity and typical velocity profiles for $\alpha = 0$ and $Re = 4$.

‡ After Roache,[2] this approach corresponds to a combination of the "Euler modified" treatment of the convection terms and the Crank-Nicholson treatment of the diffusion terms.

adopted here is similar to that already discussed. The transverse velocities at the locations above and below the x axis were then obtained through application of Eq. (18).

Results and Discussion

Plate at Zero Angle of Attack

Results were first obtained for zero angle of attack in order to gain confidence in the numerical methods adopted. Because the results of one other numerical study have been reported by Pao and Daughty[13] for this flow configuration, some comparisons are possible. A Reynolds number of 4 was chosen for these initial runs, and Δt was set equal to 0.0025.

Figure 3 shows contours of constant free vorticity at two different times. Because of flow symmetry, only results for the upper half-plane are shown. The time scale is so defined that it gives the fraction of the plate length moved by the leading edge following the impulsive start. This interpretation is exact for zero angle of attack, but it must be modified when $\alpha \neq 0$. It is evident that as time proceeds, regions of high vorticity are developed near the leading and trailing edges of the plate. These are the locations where most of the free vorticity is produced. The vorticity field is nearly symmetrical about the midcord, but there is a slight bulging of the vorticity contours in the downstream direction behind the trailing edge.

Typical profiles of u velocities are shown in the lower portion of Fig. 3. Comparison of these results (not given here) at the approximate midcord ($x = 0.025$) with those of Ref. 13 show very satisfactory agreement at the last time shown. The slight differences are probably due to the courser grid ($\Delta x = \Delta y = 0.1$) used by Pao and Daughty plus a very minor mismatching of the x and t values. They give results only for $x = 0$ and $t = 0.21$. This earlier work does not present profiles for other locations between the leading and trailing edges of the plate. Moreover, a direct comparison of velocity profiles could not be made in the regions upstream and downstream of the plate because of misalignment in the x location of nodes. Nevertheless, the basic features of the profiles computed in the present and earlier works are identical, particularly the appearance of the slight overshoot in the far-field velocity relative to the freestream value.

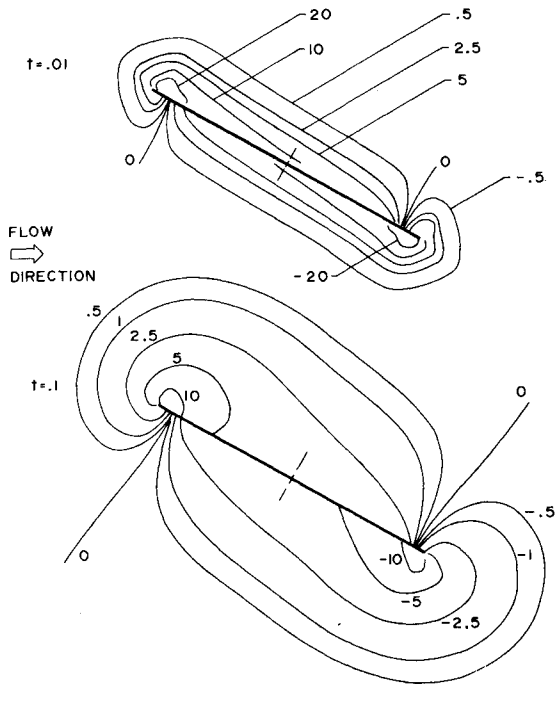

Fig. 4 Contours of constant vorticity at early times, for $\alpha = 30°$ and $Re = 4$.

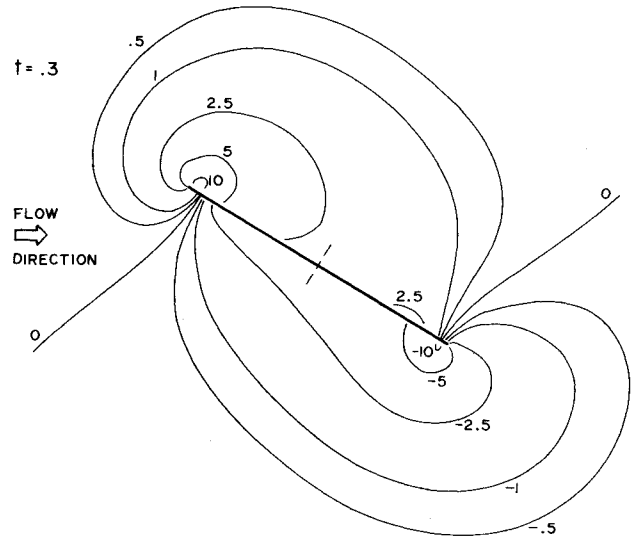

Fig. 5 Contours of constant vorticity at the last time computed for $\alpha = 30°$ and $Re = 4$.

The calculations at zero angle of attack were not carried beyond $t = 0.2$. The experience of Ref. 13 indicates that a true steady state is not reached until $t \cong 10$, although past $t \cong 2$ the results change exceedingly slowly with time. It is felt that the limited results obtained for $\alpha = 0$ in the present work generate sufficient confidence in the numerical methods to justify carrying out computations at some angle of attack, as well as at a higher Reynolds number. These latter runs offer a more demanding test of the present vorticity concepts.

Plate at Angle of Attack

Calculations have been made with $\alpha = 30°$ for Reynolds numbers of 4 and 400. The angle of attack chosen is sufficiently large to appreciably alter the flow symmetry as well as to cause significant flow reversals near the leading and trailing edges. The small Reynolds number was selected so that some comparisons could be made with the results from the previous section.

Contours of constant vorticity are shown in Figs. 4 and 5 for $Re = 4$. At the earliest time, the free-vorticity field is nearly antisymmetric about the midcord, but this appearance begins to disappear as the plate develops lift ($t = 0.3$). The contours corresponding to zero vorticity are significant since their intersection points with the plate surface identify where the wall shear

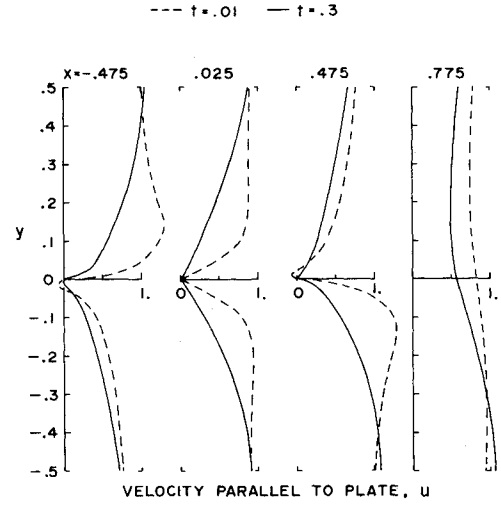

Fig. 6 Typical velocity profiles for $\alpha = 30°$ and $Re = 400$.

stress is zero. At low Reynolds number, these points are more appropriately termed flow-stagnation points rather than separation points. Examination of the velocity profiles show that near these points, the velocity boundary-layer thickness does not change abruptly, as is usually the case for separated flows at high Reynolds numbers. It appears that with increasing time, the stagnation point on the lower surface moves nearer the leading edge, whereas that on the upper surface moves nearer the trailing edge.

Typical velocity profiles at locations along the plate are shown in Fig. 6 for two different times. The profiles computed nearest the leading and trailing edges ($x = -0.475$, and $+0.475$) indicate slight reversed flow near the plate at the earlier time. However, more spatial resolution of the flow is required in these regions before the precise behavior of the velocity profiles can be studied, particularly for small time. The node point nearest the plate is 0.025 plate lengths above it.

In order to obtain results at the higher Reynolds number of 400, the y increment nearest the plate was reduced to 0.0125, but the time increment was increased to 0.005. The x increment was unchanged from 0.05.

The change in flow character at the higher Reynolds number is quite pronounced, as can be seen by comparing Figs. 5 and 7. Of significance is the fact that the point of vanishing shear on the upper surface has moved downstream to the trailing edge at the last time shown ($t = 0.2$). Also, the well-defined region of counter-clockwise vorticity downstream of the trailing edge signals the initiation of vortex shedding there. Indeed, this vorticity picture is qualitatively identical to that given by Lugt and Haussling.[8] This latter study was for a thin elliptic airfoil with $\alpha = 45°$ and $Re = 200$. Also, the earliest flow pattern shown was for $t = 1.48$. Nevertheless, it displays the same vorticity development, but at a slightly more advanced stage than that given in Fig. 7. In light of this prior work, it appears that the region of high vorticity on the upper surface near the leading edge is also the beginning of a shed vortex with clockwise rotation.

The flow behavior on the upper surface near the trailing edge is particularly interesting since it reveals how the flow tries to adjust to the expected Kutta condition as lift is developed. To examine this, velocity profiles at the location nearest the trailing edge ($x = 0.475$) are shown in Fig. 8 for several elapsed times. For a short time, the fluid definitely flows from the lower surface around the trailing edge to the top surface. The y-spacing of nodes is sufficiently small to clearly show

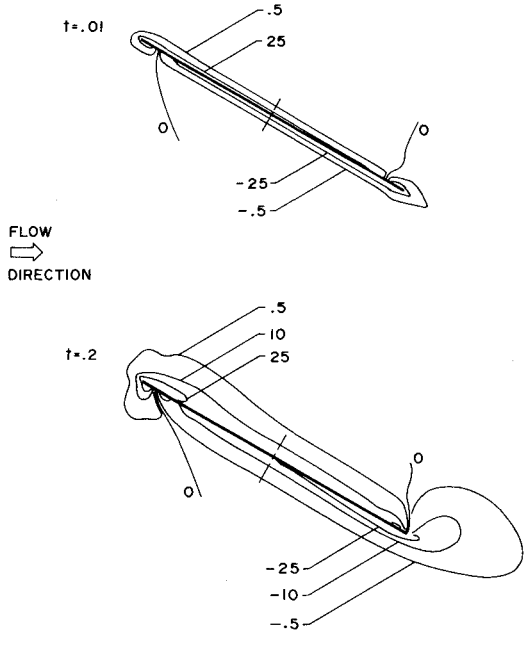

Fig. 7 Contours of constant vorticity for $\alpha = 30°$ and $Re = 400$.

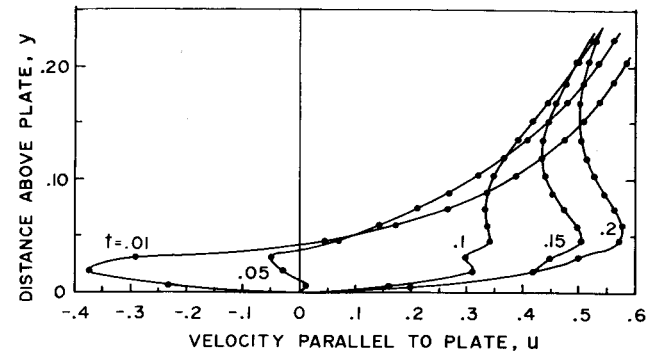

Fig. 8 Transient development of the velocity profiles on the upper surface near the trailing edge ($x = 0.475$), for $\alpha = 30°$ and $Re = 400$.

this. At $t = 0.05$, the wall shear stress is evidently positive, but there is some reversed flow above the plate. This effect disappears as time progresses, and at $t = 0.2$ the flow appears to be leaving smoothly from the trailing edge. This behavior lends strong support to the present computational scheme, particularly as it relates to the calculation of K and the spatial distribution of the bound vorticity along the plate. Also, it illustrates that computational difficulties are not encountered in regions of reversed flow.

Conclusions

Concepts which are well established for inviscid aerodynamics have been extended to the study of unsteady viscous flows. The basic philosophy has been to replace the solid aerodynamic shape with appropriate distributions of sheet and bound vorticity. These are so constituted that the fluid adherence condition is satisfied at the solid surface. The vortex sheets, which reduce the tangential slip to zero, act as surface sources and sinks of free vorticity. This enters the fluid by transverse diffusion and is ultimately distributed throughout the entire viscous flow. The resulting surface boundary condition is thus quite different from that used in conventional numerical studies of two-dimensional flows. It has long been recognized that all of the fluid vorticity in incompressible two-dimensional flows is generated at solid surfaces. The phenomenological description of the mechanism for this has previously been given by Lighthill.[3] However, the present work is believed to be one of the first to use this as the basis for a computational routine.

The relationship between vorticity and velocity (Biot-Savart Law) is most familiar to those dealing with inviscid flows. Nevertheless, it is purely kinematical and is therefore applicable to viscous flows as well. Indeed, the results presented in the foregoing sections correspond to fully numerical solutions to the complete Navier-Stokes equations in two dimensions. The advantage of the integral relationship is that it allows the velocity field to be computed directly from the vorticity distributions and thus avoids the usual iterative schemes associated with stream-function methods.

References

[1] *Proceedings of the AIAA Computational Fluid Dynamics Conference*, Palm Springs, Calif., July 19–20, 1973.

[2] Roache, P. J., *Computational Fluid Dynamics*, Hermosa Publishers, Albuquerque, N. Mex., 1972.

[3] Lighthill, M. J., "Introduction. Boundary Layer Theory," *Laminar Boundary Layers*, edited by J. Rosenhead, Oxford University Press, New York, 1963, pp. 54–61.

[4] Paolino, M. A., "Vorticity Models for Predicting Transient Flow Phenomena," Ph.D. thesis, 1972, Univ. of Arizona, Tucson, Ariz.

[5] Kinney, R. B. and Paolino, M. A., "Flow Transient Near the Leading Edge of a Semi-Infinite Flat Plate Moving Through a Viscous Fluid," presented at the Seventh U.S. National Congress of Applied Mechanics, University of Colorado, Boulder, Colo., June 3–7, 1974; also *Transactions of the ASME, Journal of Applied Mechanics*, to be published.

[6] Wu, J. C. and Thompson, J. F., "Numerical Solution of Time-Dependent Incompressible Navier-Stokes Equations Using an Integro-Differential Formulation," *Computers and Fluids*, Vol. 1, No. 2, 1973, pp. 197–215.

[7] Chorin, A. J., "Numerical Study of Slightly Viscous Flow," *Journal of Fluid Mechanics*, Vol. 57, 1973, pp. 785–796.

[8] Lugt, H. J. and Haussling, H. J., "Laminar Flow Past a Flat Plate at Various Angles of Attack," *Proceedings of the Second International Conference on Numerical Methods in Fluid Dynamics*, Springer-Verlag, New York, 1970, pp. 78–83; also Rept. 3748, Feb. 1972, Naval Ship Research and Development Center, Bethesda, Md.

[9] Batchelor, G. K., "The Source of Vorticity in Motions Generated from Rest," *An Introduction to Fluid Dynamics*, Cambridge University Press, Cambridge, 1970, pp. 277–282.

[10] Karamcheti, K., "Elements of Thin Airfoil Theory," *Principles of Ideal-Fluid Aerodynamics*, Wiley, New York, 1966, pp. 492–517.

[11] Gentry, R. A., Martin, R. E., and Daly, B. J., "An Eulerian Differencing Method for Unsteady Compressible Flow Problems," *Journal of Computational Physics*, Vol. 1, 1966, pp. 87–118.

[12] Schmall, R. A., "Unsteady Viscous Flow Past a Lifting Plate," Ph.D. thesis, 1974, Univ. of Arizona, Tucson, Ariz.

[13] Pao, Y.-H. and Daughty, R. J., "Time-Dependent Viscous Incompressible Flow Past a Finite Flat Plate," Rept. D1-82-0822, Jan. 1969, Boeing Scientific Research Labs., Seattle, Wash.

NOVEMBER 1974 AIAA JOURNAL VOL. 12, NO. 11

When is Hamilton's Principle an Extremum Principle?

DONALD R. SMITH*
University of California, San Diego, Calif.
AND
C. V. SMITH JR.†
Georgia Institute of Technology, Atlanta, Ga.

For a dynamic system, the action I for motion from time t_0 to time t_1 can be written as $I = \int_{t_0}^{t_1}(T-V)\,dt$, where T is the kinetic energy and V is the potential energy. In many references to Hamilton's principle, particularly in the engineering literature, it is stated or implied that the true motion of the system will give the action an extreme value, usually stated to be a minimum value. In this Paper it is first demonstrated by very simple examples that Hamilton's principle is not, in general, an extremum principle. Then a relatively elementary and direct proof, which does not require sufficiency theory from the calculus of variations, is presented which shows that for certain discrete linear systems the action is always minimized over short time intervals; and a precise characterization is given for the maximum length of the time interval over which the action is guaranteed to be minimized by the true solution. Finally, it is shown that for continuous systems the action is never minimized by the true solution.

Introduction

FOR the restricted but commonly occurring problem of determining the motion of a conservative system, Hamilton's principle states that the true motion between time t_0 and time t_1 will be such as to satisfy the following equation:

$$\delta \int_{t_0}^{t_1} (T-V)\,dt = 0 \tag{1}$$

where T = kinetic energy of the system and V = potential energy of the system. This equation is presented in texts from mathematics,[1–4] physics,[5] structural mechanics,[6] and structural dynamics[7]; and in most references it is stated that the true solution not only makes the quantity

$$I = \int_{t_0}^{t_1} (T-V)\,dt \tag{2}$$

(called the action of the motion) stationary but also gives I an extremum value, usually stated to be a minimum value. For example, in Ref. 2, it is stated that the actual motion "makes the functional $\int_{t_0}^{t_1}(T-U)\,dt$ a minimum." In Ref. 7 it is said, "The stationary value is actually a minimum." Or in Ref. 5, "...out of all possible paths by which the system point could travel from its position at time t_1 to its position at time t_2, it will actually travel along that path for which the integral...is an extremum, whether a minimum or maximum...."

Only a relatively few references,[1,3,4] generally in the literature of the calculus of variations, give the more precise statement of Hamilton's principle in which it is recognized that the action is possibly minimized only over short intervals of time. Reference 3 contains a brief treatment of one example in which an alternate form of the action integral is not minimized by a true solution over long intervals of time. (However, for that example if the action is defined as given in Eq. (2), then any true solution minimizes the action for all intervals of time.)

In this paper it will be demonstrated by both example and proof that in general Hamilton's principle for conservative systems is not an extremum principle. This will be accomplished by considering the free vibration of linearly elastic systems. Then it will be shown that for discrete linear systems, "in fact, the action is always minimized over short time intervals..." as stated in Ref. 1, and a precise characterization will be given for the maximum length of the time interval over which the action can be guaranteed to be minimized by the true solution. Finally, for continuous systems it will be shown that the action is never minimized by the true solution.

It should be noted that these results, while evidently not well-known in engineering literature, are available in Ref. 4, where

Received January 28, 1974; revision received June 24, 1974.
Index categories: Structural Dynamic Analysis.

* Associate Professor, Department of Mathematics.
† Associate Professor, School of Aerospace Engineering. Member AIAA.